Journal of Rehabilitation in Civil Engineering 13-2 (2025) 218-242

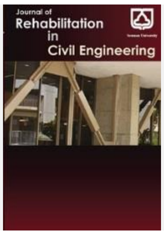

Journal of Rehabilitation in Civil Engineering

Journal homepage: https://civiljournal.semnan.ac.ir/

Seismic Microzonation and Probability of Ground Failure Assessment Caused by liquefaction for Bogura District, Bangladesh

Md. Belal Hossain [1]; Md. Mahabub Rahman [2,*]

1. Associate Professor, Department of Civil Engineering, Hajee Mohammad Danesh Science and Technology University, Bangladesh
2. Lecturer, Department of Civil Engineering, Hajee Mohammad Danesh Science and Technology University, Bangladesh
* Corresponding author: *mmr.civil@hstu.ac.bd*

ARTICLE INFO

Article history:
Received: 18 May 2024
Revised: 10 August 2024
Accepted: 31 October 2024

Keywords:
Seismic zonation;
Ground failure probability;
SPT data;
Bogura;
Hazard map.

ABSTRACT

The aim of this study is to create a Mercalli intensity map and evaluate the ground failure probability caused by liquefaction in the Bogura district. To generate a Mercalli intensity seismic microzonation map, first the shear wave velocity (Vs) was determined by analyzing data from 345 soil test reports. The conversion of Vs to site amplification factor (AF) and Peak Ground Acceleration (PGA) was carried out using the widely used empirical equations, considering earthquake magnitudes 1850–2023. Finally, the susceptibility of liquefaction was evaluated for the study area using 345 borehole data, considering a probable earthquake magnitude and site-specific PGA. Some of the frequently used empirical methods are utilized for the evaluation, and the results are presented in the form of hazard maps indicating factors of safety, liquefaction potential, and ground failure probability. The results demonstrate that the least and maximum PGA are both 0.06 g and 0.16 g, while the AF ranges from 1.903 to 3.98 between the minimum and maximum. Moreover, the surface acceleration (SA) varies between 0.143 g and 0.51 g. Based on the Mercalli Intensity seismic microzonation map, 22.45% of the areas have intensity VII, 72.9% of the regions have intensity VIII, and 4.65% of the areas have intensity IX. The hazard map reveals that 2% of the study region is judged to be at extremely high risk for ground failure due to liquefaction during the scenario earthquake. Additionally, it was determined that 13% and 44% of the study region's regions were at high or moderate risk of ground failure under the aforementioned earthquake scenario. The intensity and hazard maps created for Bogura district are crucial to achieving sustainable development goals.

E-ISSN: 2345-4423

How to cite this article:
Hossain, M. B., & Rahman, M. (2025). Seismic Microzonation and Probability of Ground Failure Assessment Caused by liquefaction for Bogura District, Bangladesh. Journal of Rehabilitation in Civil Engineering, 13(2), 218-242. https://doi.org/10.22075/jrce.2024.34111.2086

1. Introduction

The preliminary stage in a seismic risk mitigation study is seismic micro-zonation. It necessitates a multidisciplinary strategy that includes significant insights from geology, seismology, and geotechnical engineering [1]. Using geologic and geotechnical data, which may identify, regulate, and prevent geological risks, is becoming increasingly important in micro-zonation, particularly in the development of urban infrastructure [2,3]. There are three basic stages of seismic micro-zonation studies: establishing the local geological and geotechnical site characteristics, evaluating probable ground reaction, and analyzing factors relating to ground motion on the surface. Seismic micro-zonation is considered to split a territory into discrete zones with varied possible hazardous earthquake impacts. Also characterizing their particular seismic susceptibility for the design of infrastructure and planning for land use [4,5]. Micro-zonation is a widely used approach in earthquake risk and hazard assessment. It can be defined as the categorization of ground motion parameters, taking into account source and field circumstances [4]. Seismic vulnerability and performance were assessed by different researchers around the world. There are various types of structure like steel fame [6,7], RC frame [8,9], oldest masonry structures [10] were analyzed under seismicity.

Liquefaction is a secondary potential danger caused by seismic loading, with earthquakes being the primary hazard. It is a technique by which soil sediments beneath the water table momentarily lose their strength and act like viscous fluids [11]. In general, saturated sandy soils settle and become packed when subjected to seismic loading. However, the existence of pore water in the void space causes a rise in pore pressure, which rises gradually with each cycle of loading, causing the soil to lose shear strength and stiffness and thus drawing liquefaction [12]. In previous decades, liquefaction-induced geological and structural damage has been recorded in several places around the world *in* loose, submerged sands and other gravelly soils [13]. For instance, the devastating effects of major earthquakes, such as the incidence of soil liquefaction at numerous places, were replicated in the 2010 Chilean earthquake [14]. In addition, several liquefaction-related structure collapses were seen after Japan's 2016 Kumamoto earthquake [15]. Also, several damages were caused by liquefaction in the Emilia-Romagna earthquake in 2012 and the Gorkha earthquake in 2015 [16]. To reduce these structural damages, various researchers around the world assess soil liquefaction in specific regions. The researchers used cone penetration test data and SPT data to determine liquefaction numerically [17–19]. In recent days, machine learning has been a new approach to evaluating this catastrophic event [20–22]. Like soil liquefaction, other geohazards like land slide risk assessment and slope collapse analysis are also crucial to reducing losses during earthquakes [23,24]. The previous research findings have provided a significant understanding of the circumstances that promote liquefaction, including fine, loose, and saturating silty sands, low-plastic silty clays, and non-plastic silts, where a considerable decline in shear strength occurs [25]. In addition, it has been found that moderate earthquakes (Mw = 5 to 6) as well as earthquakes with a high magnitude (Mw > 7) can cause liquefaction [26]. Bogura is the most important northwest district of Bangladesh. This area's population has risen at least 50 times since the turn of the century. It has 2926 grid points that are 1 km by 1 km and has a population of more than a million (Fig. 1). The geological location of this area makes it prone to earthquakes. The Bogura area has had about 21 large earthquakes with magnitudes that varied from 5 to 7.14 over the preceding 108 years. Although the Bogura district is seismically vulnerable, there is no Mercalli intensity risk map for seismic activity. GIS may be effectively used to create spatial distribution maps using various interpolation techniques [27]. Previous researchers find more accuracy to using GIS in mapping groundwater and landslide susceptibility mapping [28,29].

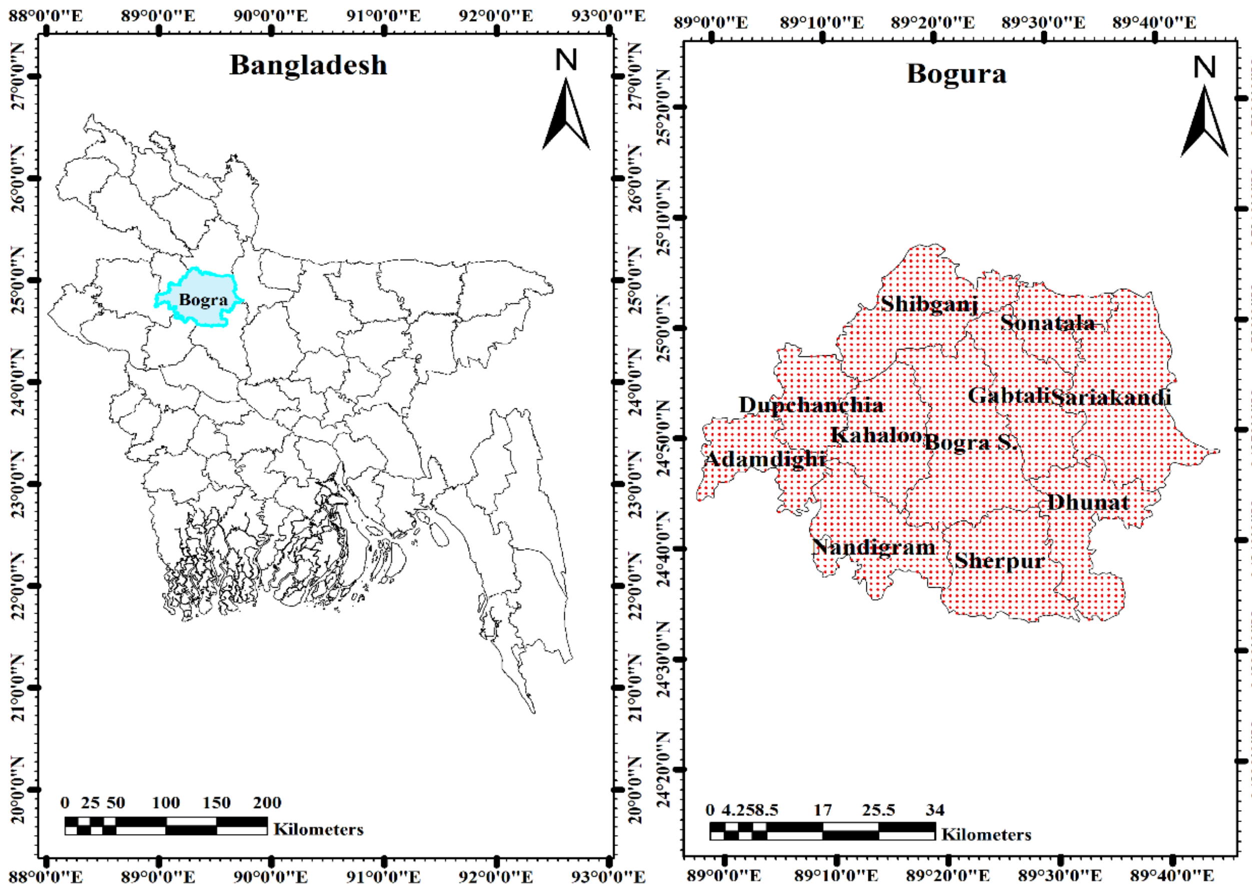

Fig. 1. Research area (grid dimension 1 km x 1 km).

The purpose of this research is to produce an intensity map using universally applicable equations and GIS for the Bogura district. This is accomplished by calculating the Vs using data from 345 boreholes. Since the determined Vs from the SPT-N value gathered from the boring log data was 15 meters deep, it was then converted up to a depth of 30 meters. To convert Vs to the site AF, the McGuire [30] and "Atkinson and Boore" [31] equations are utilized. The PGA is also computed using the McGuire equation, considering earthquakes 1850–2023. Using the equation with the biggest AF between the two, the PGA was transformed into the SA. Finally, the SA has been transformed into the Modified Mercalli Intensity (MMI) scale to facilitate understanding.

Furthermore, this research is the first to evaluate the PG in the Bogura District as a result of soil liquefaction. This area has a large risk of liquefaction brought on by earthquakes because of its alluvial soil, high groundwater table, and placement in an earthquake-prone area. The region's susceptibility to liquefaction hasn't been investigated, though. Therefore, to provide trustworthy urban development, a liquefaction hazard evaluation for the metropolis is required. The vulnerability of liquefaction phenomena in the subsurface layer of the study region is calculated in terms of FOS and LPI. Idriss and Boulanger [32] are utilized to determine FOS, and Iwasaki et al. [33] are utilized to calculate LPI. This analysis is conducted by taking into account an earthquake magnitude of Mw = 6.5 with an estimated site-specific PGA value. Then PG is determined from LPI, utilizing an empirical approach proposed by Li et al. [34]. Finally, all the numerical values are used to produce spatial distribution maps using ArcGIS software.

2. Study area

2.1. General

The city of Bogura, also called Bogra, is located in the northwestern part of Bangladesh in the Bogura District, in the fertile Bengal Delta region, which is the largest in the district. A major component of Bogura city's geomorphology is shaped by natural processes occurring along the Ganges-Brahmaputra-Meghna (GBM) river system.

2.2. Geomorphology

A Following are detailed descriptions of the soil classification in Bogura District based on a digital soil map developed by the Food and Agriculture Organization (FAO). A soil classification map for Bogura district is shown in Fig. 2. The map indicates that Bogura is primarily covered by four soil types. These soil types include alluvial silt, alluvial sand, alluvial silt and clay, and clay residue. Alluvial sand covers 6% of the total area in Bogura district. Approximately 32% of Bogura district is covered by alluvial silt. These fine particles are smaller than sand but larger than clay. Out of the total area of Bogura district, 12% is covered with this type of soil. Alluvial silt and clay soils tend to be smooth, cohesive, and may exhibit some stickiness when wet [35]. Clay residuum refers to a type of soil formed directly from the weathering and decomposition of parent rock material without significant transport or deposition. In the case of Bogura district, 44% of the area is covered with this type of soil.

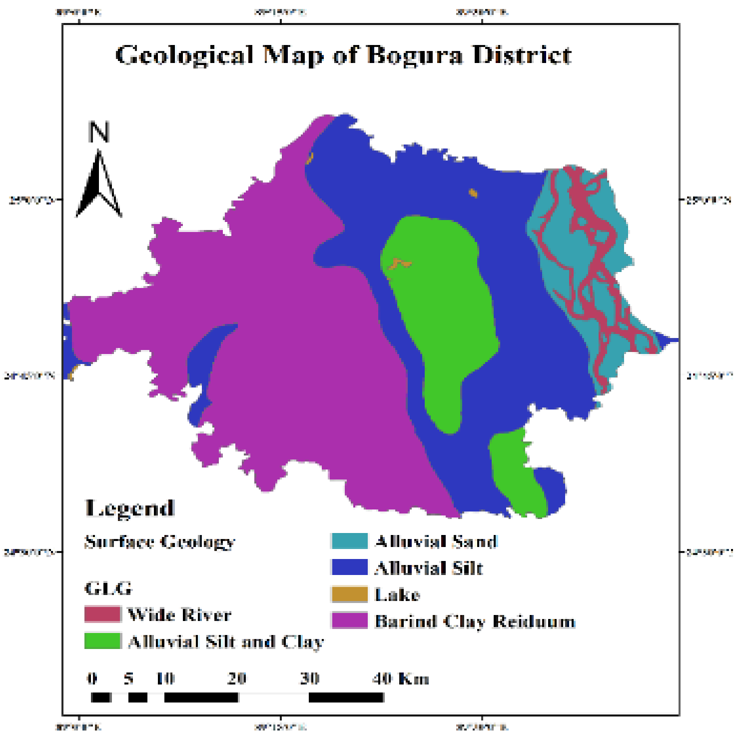

Fig. 2. Surface geology of Bogura created by FAO.

2.3. Seismicity

Fig. 3. shows that Bangladesh is bounded by many different kinds of geological blocks that have caused numerous earthquake events in the past few years [32]. In terms of geology and plate

tectonics, five key faults are important for the occurrence of destructive earthquakes. Among them the Bogra fault is a kind of gravity fault. It is extremely near to the town of Bogra and the Jamuna River. The deposition of a substantial volume of sedimentary material within the Bogra graben was caused by displacement along the Bogra fault [36]. Bogura District is generally considered seismically moderate vulnerable. The district is situated away from major tectonic plate boundaries, which are typically associated with high seismic activity.

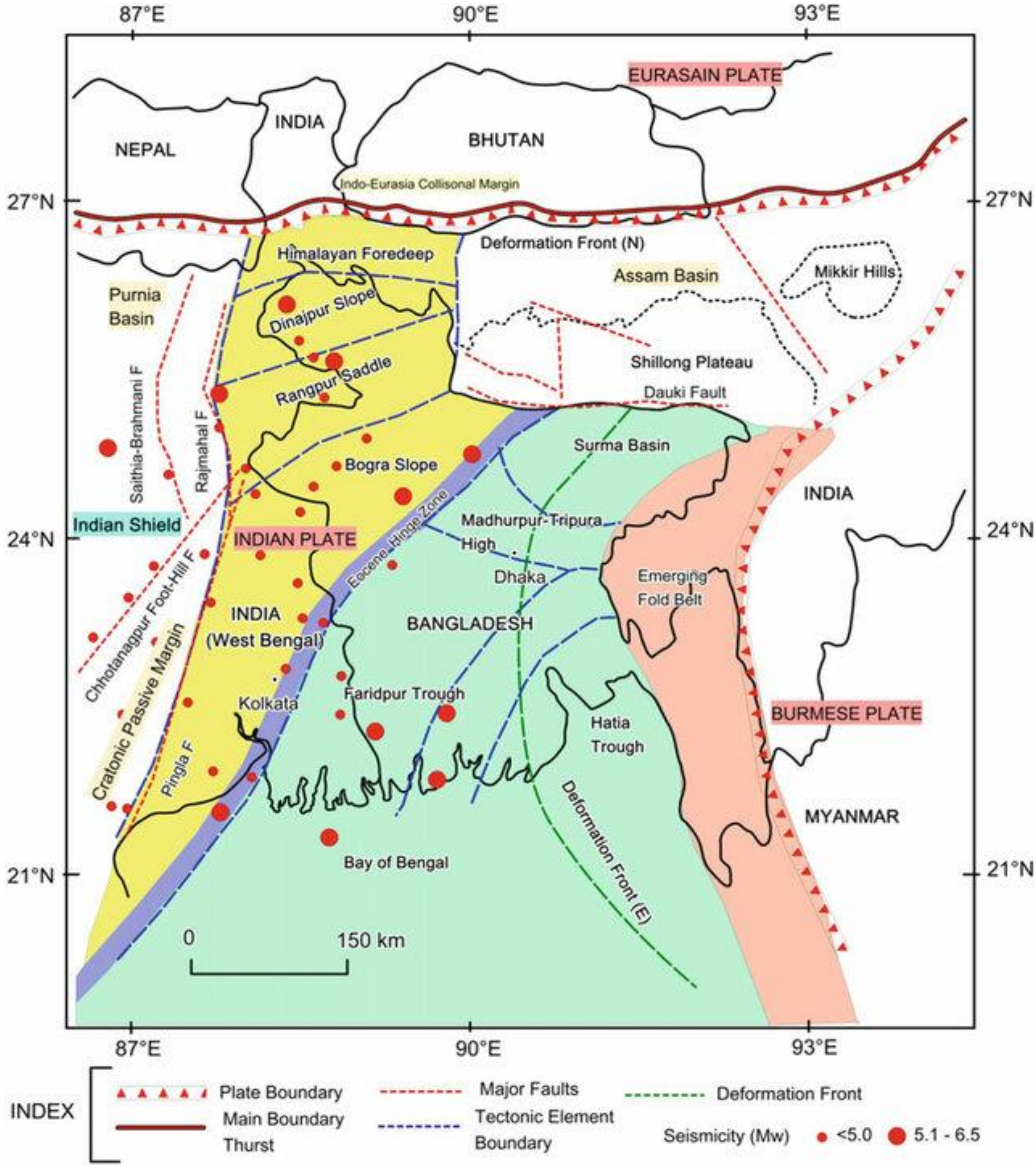

Fig. 3. Bangladesh with tectonic elements, faults, and seismicity (Mw > 4) [37].

As a result, Bogura District experiences relatively moderate seismicity compared to other regions prone to earthquakes. However, it is important to note that Bangladesh as a whole lie in a seismically active zone, known as the Bengal Basin. In seismic zonation map Bogura district is categorized in zone 3 with zone coefficient 0.28 [38]. Historical seismic data indicates that Bogura District has experienced occasional low to moderate seismic events, typically with magnitudes ranging from 4 to 5 on the Richter scale. Considering the low to moderate seismicity of the region, the structural integrity of buildings and infrastructure in Bogura District is not typically designed to withstand high-intensity earthquakes. However, local construction practices have improved over time, with increasing awareness of seismic risks in the country.

2.4. Geotechnical conditions

The potential for liquefaction can be estimated by considering the properties of subsurface present in a particular region [39]. For this research, a dataset consisting of 345 borehole data points with standard penetration tests (SPT) was employed. Among these, ten boreholes were specifically tested by a private company to acquire precise information about the study area. The remaining data were gathered from geotechnical investigation reports of 335 locations within the study area, which were conducted by different government and local private laboratories. The geotechnical investigation reports collected for this study involved various test results. These are SPT, particle size analyses, Atterberg's limits, unit weight, and triaxial tests etc. Statistical analysis was conducted to assess the variability of the data, including the calculation of the number of data points (n), minimum and maximum values, mean value (μ), standard deviation (σ), and coefficient of variation (COV). These results are presented in Table 1.

Table 1. Statistical analysis of the geotechnical characteristics.

Descriptive statistics	SPT	FC (%)	LL	PL	PI
Mean	19	44.04	44.7	17.0	27.68
Median	15	30	45	17	28
Mode	10	20	46	16	30
Standard Deviation	12.76	29.16	1.40	1.17	2.44
Kurtosis	-0.52	-1.65	1.52	5.34	0.85
Skewness	0.75	0.31	-1.2	0.14	-0.78
Minimum	0	3	40	10	20
Maximum	50	95	48	24	36
COV (%)	66.56	66.23	3.13	6.88	8.83
Count	1452	1293	624	624	624

Additionally, Fig. 4a-c illustrates the variation of geo-technical parameters with depth. Fig. 4a reveals that approximately 60.8% of the borehole exhibit N values that are below 20, while over 35% of the locations have N values less than 10, particularly at shallow depths. Additionally, the average SPT-N values for the soil in the study area at depths of 1.5 m, 3 m, 6 m, 9 m, and 12 m are 8, 10, 16, 26, and 35, respectively. Similarly, Fig. 4c shows how the fine content (FC) of Bogura soils varies with depth. The FC values have a mean of 44.04 and the range of the FC values is from 3 to 95%. This suggests that low FC is present in shallow depths over a significant portion of the research region.

The plasticity index (PI) values for the majority of the soils in the research region lie between 20 and 36%, as shown by Fig. 4b (mean = 27.68, standard deviation = 2.44, and coefficient of variation = 8.83%). According to Table 1, the LL and PI mean values are determined to be 44.72% and

27.68%, respectively, which amply demonstrates the presence of medium-plasticity soils in the studied region. It's interesting to note that the research area's soil liquefaction susceptibility is supported by the study area's lower SPT-N value, the abundance of cohesionless soils with low fines content.

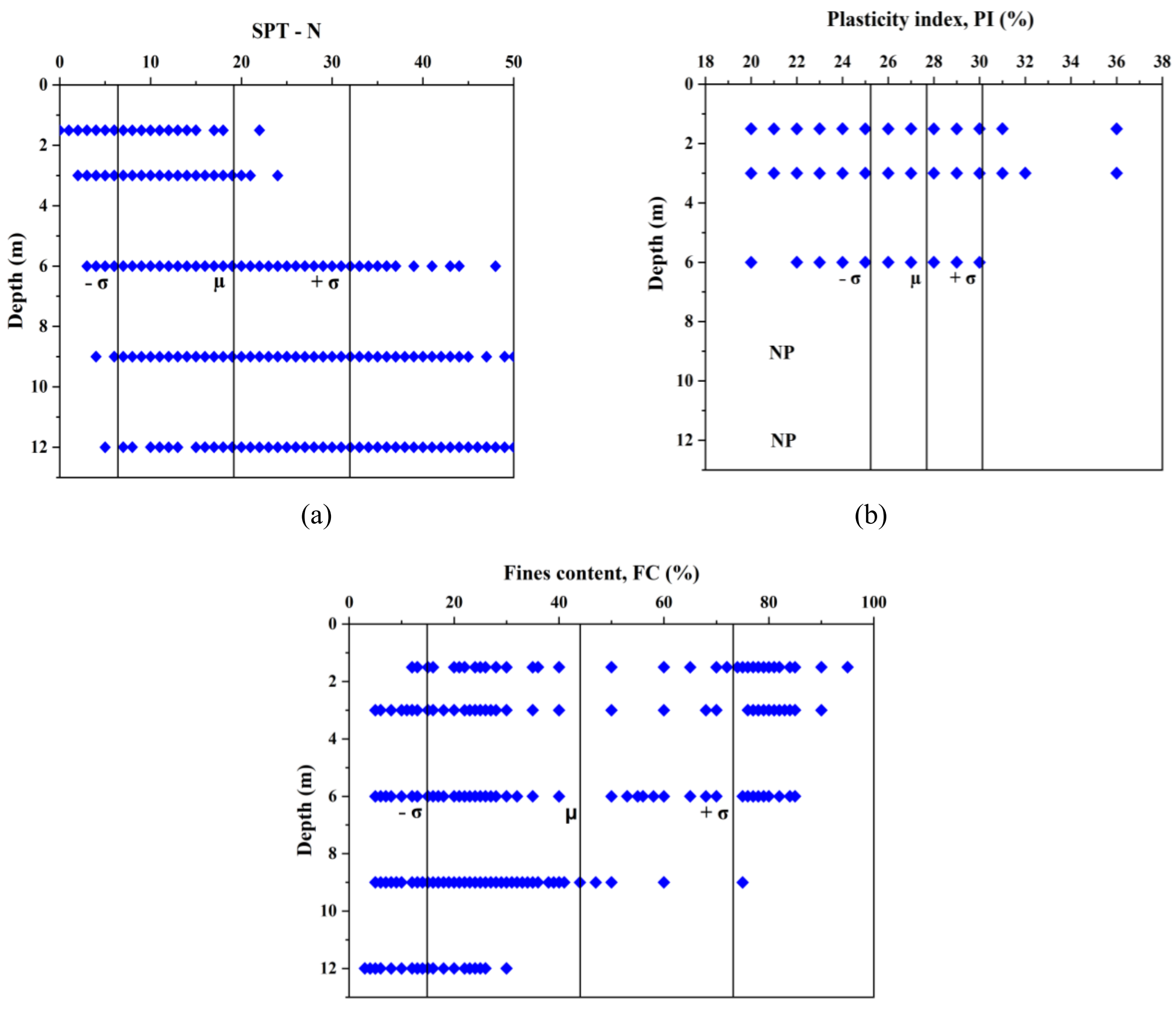

(c)

Fig. 4. Depth wise variation of (a) SPT-N, (b) plasticity index (PI), and (c) fines content (FC) showing standard deviation (σ) and mean (μ) of the data.

2.5. Hydrological conditions

Groundwater plays a serious role in the phenomenon of soil liquefaction and the swelling of fine sediments [40]. Groundwater at higher elevation increase the likelihood of liquefaction occurring during an earthquake [41]. Fig. 5 displays a geographical map of the research region that displays the ground water level.

The interpolation map of GWT depicts that approximately 88.96% of the borehole locations had a GWT ranging from 0.15-4.5. More than 50 % had a GWT ranging from 0.15- 3. This indicates that the Bogura district is vulnerable to liquefaction during seismic events.

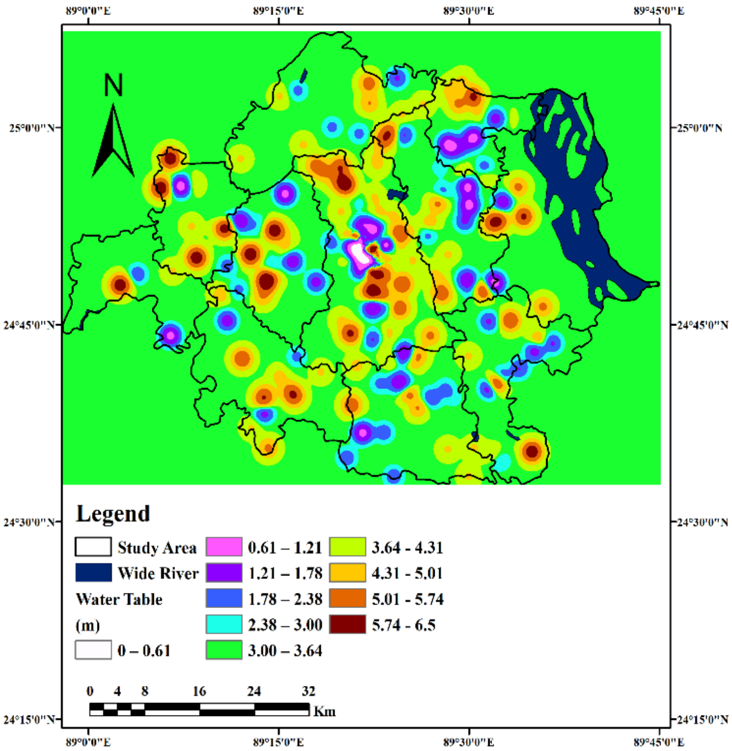

Fig. 5. Groundwater spatial mapping produced from borehole data.

3. Methodology

3.1. Seismic micro-zonation

To evaluate the seismic hazard and intensity at every site, an attenuating law for PGA is necessary. Since the soil in Bangladesh is like the type of soil used in the McGuire legislation and the MMI values could be attained with some transformation, the attenuation law of McGuire [42] was used in this study. Fig. 6 shows the flowchart of seismic zonation analysis.

3.1.1. Estimation of Vs from SPT

There are numerous empirical equations that can be utilized to compute the Vs from uncorrected SPT-N. Three empirical equations from Lee [43] are applied in this work since other Eqns. attempt to focus on a single relationship between uncorrected N and Vs. However, Lee focused on different soil types and proposed Eq. 1 for sand, Eq. 2 for sand silt, and Eq. 3 for sand clay [44].

$$V_s = 57.4\, N^{0.49} \quad (1)$$

$$V_s = 105.64\, N^{0.32} \quad (2)$$

$$V_s = 114.43\, N^{0.31} \quad (3)$$

Where, N is obtained from field test.

3.1.2. Evaluation of Vs (< 30m)

The determined Vs was up to a depth of 30 meters. Therefore, by utilizing the mean Vs of 15 meters and employing Boore's law (Eq. 4), it is possible to compute the Vs at a depth less than 30 meters [45][46].

$$\log \bar{V}_s\,(30) = a + b \log \bar{V}_s(d) \quad (4)$$

Where, a and b are regression factor. $a = 0.013795$ and $b = 1.0263$ for 15m depth [47].

$\bar{V}_s$(d) = Vs average value up to 15m

3.1.3. Estimation of PGA

A PGA attenuation law has not been created for Bangladesh due to a lack of strong-motion data. In this investigation, the McGuire attenuation [42] was used since the land in Bogura district is like the land to which the McGuire legislation applies [48]. The relationship is as follows (Eq. 5).

$$y = 0.0306\, e^{0.89}Mr^{-1.17}e^{-0.2s} \tag{5}$$

In the above equation, $y = PGA$, M = magnitude of surface wave, s = 0 (rock) and s=1 (alluvial), r = Hypo central distance $=\sqrt{d^2 + h^2}$, d = epicenter to location distance, h = focal depth.

3.1.4. Estimation of AF

In places where Vs profiles are available, the site AF is calculated using Eq. 6 [49], the relationships between the average shear wave velocity (AVS_{depth}) and AF is-

$$\log(AF) = -0.734 \times \log(AVS_{depth}) + 1.98 \tag{6}$$

The following Eq. 7 is used to calculate the AVS_{depth}.

$$AVS_{depth} = \frac{d}{\sum_{i=1}^{n} \frac{h_i}{v_i}} \tag{7}$$

Where, the variable "h_i" represents the layer thickness (m), while depth is "d" and "v_i" represents the Vs of i_{th} layer out of a total of n layers present at that depth. Eq. 6 calculates the AF, which is generally lower than the AF obtained from another equation. However, in certain exceptional situations, Eq. 6 yields higher values. A second equation created by Boore and Atkinson [50] is used to determine the AF. Only shear wave velocities at depths of less than 30 m are appropriate for the AF provided by this equation. Only linear amplification is considered in this analysis since, at low PGA, the nonlinear term does not change compared to the linear term. The following Eq. 8 measures the factor.

$$\ln AF = c * \ln\left(\frac{V_{s30}}{V_{ref}}\right) \tag{8}$$

For Bogura, Characteristic site period is about 0.313–0.688. Because of the poorer conditions at the site that corresponds to the deeper site, the c value for this study is chosen for a time of 0.5 s. So, the value of $c = -0.9384$ and $V_{ref} = 760\ m/s$ [50].

3.1.5. Estimation of SA

The PGA value is multiplied with AF to obtain the surface acceleration.

$$SA = PGA * AF$$

3.1.6. Conversion of PGA to MMI

SA and MMI connection are being developed by Trifunac and Brady [51]. The MMI is calculated using the following Eq. 9.

$$\log PGA_s = 0.014 + 0.3(MMI) \tag{9}$$

where, PGA_s refers to the surface's PGA.

3.2. Determination of earthquake magnitude parameters

The evaluation conducted in this research provided site-specific maximum ground accelerations, called PGAs, for the research region. In assessing liquefaction vulnerability, these PGAs as well as an estimated earthquake magnitude were taken into account. The liquefaction vulnerability for the research region is assessed in terms of FOS, LPI and PG. As stated in the sections below, these parameters were derived using conventional methods. In ArcGIS, the resultant data were interpolated using the Kriging interpolation and shown as risk zonation maps in terms of the FOS, PG, and LPI. Moreover, graphical and statistical visualizations were prepared using OriginPro.

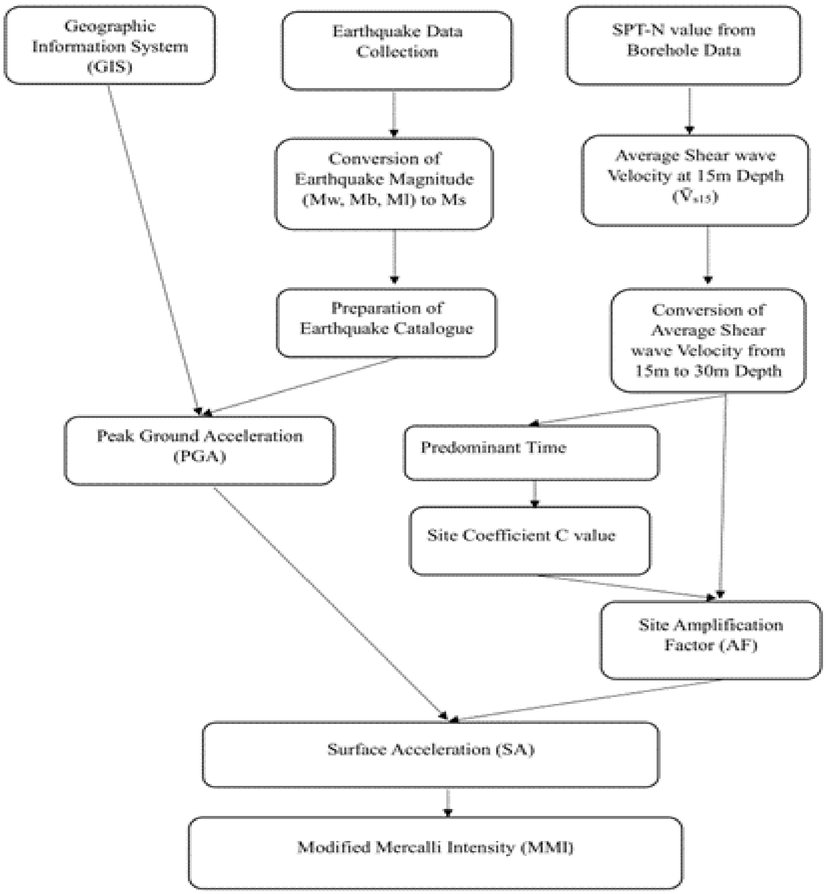

Fig. 6. Flowchart of seismic analysis.

3.2.1. Determination of the FOS

In this investigation, FOS is determined by the Eq. 10 discovered by Idriss and Boulanger [32]. The framework specifies the cyclic resistance ratio (CRR) of the soils, and the cyclic stress ratio (CSR) is the stress (loading) generated in the ground as a result of a design seismic event that causes liquefaction.

$$\mathrm{FOS} = \frac{\mathrm{CRR}_{7.5}}{\mathrm{CSR}} * \mathrm{MSF} * \mathrm{K}_{\sigma} \tag{10}$$

Where, $CRR_{7.5}$ is the CRR calibrated for an earthquake with Mw = 7.5. Additionally, the magnitude scaling factor (MSF) is incorporated to account for the influence of shaking duration, while the factor K_σ is sustained static shear stresses. The values of MSF and K_σ were determined using Eq. 11 and Eq. 12, respectively.

$$MSF = 6.9e^{\frac{-M_w}{4}} - 0.058\ (\leq 1.8) \tag{11}$$

$$K_\sigma = 1 - C_\sigma \ln(\frac{\sigma_v{}'}{P_a})\ (\leq 1.1) \tag{12}$$

In the above equation, C_σ can be obtained by Eq. 13.

$$C_\sigma = \frac{1}{18.9 - 2.55\sqrt{(N_1)_{60}}}\ (\leq 0.3) \tag{13}$$

The CRR was calculated using the N value corrected by field procedure and overburden pressure, and the uncorrected SPT-N value was corrected using Eq. 14.

$$(N_1)_{60} = NC_N C_E C_B C_R C_s \tag{14}$$

Where, $(N_1)_{60}$ is adjusted field N value. N is obtained from field. C_N, C_B, C_E, C_R, and C_S are the correction factors for overburden stress, borehole diameter, type of hammer used, rod length, and type of samplers used, respectively.

The $CRR_{7.5}$ is assessed using Eq. 15.

$$CRR_{7.5} = \exp\left(\frac{(N_1)_{60cs}}{14.1} + \left(\frac{(N_1)_{60cs}}{126}\right)^2 + \left(\frac{(N_1)_{60cs}}{23.6}\right)^3 + \left(\frac{(N_1)_{60cs}}{25.4}\right)^4 - 2.8\right) \tag{15}$$

In Eqn. 15, $(N_1)_{60cs}$ stands for soil fines content correction.

Eq. 16 and Eq.17 are used to calculate $(N_1)_{60cs}$:

$$(N_1)_{60cs} = (N_1)_{60} + \Delta(N_1)_{60} \tag{16}$$

$$\Delta(N_1)_{60} = \exp\left(1.63 + \frac{9.7}{FC+0.01} - \left(\frac{15.7}{FC+0.01}\right)^2\right) \tag{17}$$

In the above equation, FC represents the finer percent. The CSR is then computed using Eq. 18.

$$CSR = 0.65\frac{\tau_{max}}{\sigma'_v} = 0.65\frac{a_{max}}{g}\frac{\sigma_v}{\sigma_v{}'}r_d \tag{18}$$

Where, 'a_{max}' denotes the PGA, 'g' represents gravitational acceleration, σ_v and $\sigma_v{}'$are the total and effective overburden stress, respectively, and r_d is the stress reduction factor as given in Eq. 19.

$For, z \leq 34m,$

$$rd = \exp[\alpha(z) + \beta(z)M] \tag{19}$$

In the above equation,

$\alpha(z) = -1.012 - 1.126\, sin[(z\ /\ 11.73) + 5.133]$

$\beta(z) = 0.106 + 0.118\, sin[(z\ /\ 11.28) + 5.142]$

$For, z > 34m,$

$rd = 0.12\, exp\ (0.22M)$

Where ‘z’ is the soil layer thickness (m) and M is the magnitude of the earthquake.

3.2.2. Estimation of the LPI

The LPI at the desired locations is calculated by Iwasaki et al. [33]. The LPI is assessed by Eq. 20 up to a depth of 20 m or less of soil layer from the ground surface.

$$\mathrm{LPI} = \int_0^{z} \mathrm{F(z)W(z)dz} \tag{20}$$

where z = layer thickness; F(z) = function of FOS and obtained by:

when $FOS \leq 1$ then $F(z) = 1$

when $FOS > 1$ then $F(z) = 0$

In the above equation, W(z) is a factor determined by Eq. 21:

$$\mathrm{W\,(z)} = 10 - 0.5\mathrm{z} \tag{21}$$

According to the LPI value, the susceptibility to liquefaction can be categorized into four distinct groups: extremely low, low, high, and extremely high.

3.2.3 Evaluation of PG

To conduct a quantitative assessment, the possibility of ground failure caused by liquefaction (referred to as PG) was determined using Eq. 22 as presented in reference [34].

$$\mathrm{P_G} = \frac{1}{1+\mathrm{e}^{4.71-0.71*\mathrm{LPI}}} \tag{22}$$

where LPI represents the liquefaction potential, can be calculated using Eq. 11.

4. Results and discussion

4.1. Seismic hazard and intensity

In field investigation, the SPT number and the estimation of the V_s are very important parameters. The V_s is used to determines the mechanical characteristics of any soil [52]. In order to determine the V_s in-situ testing is always preferable for accurate result. However, the necessary equipment’s required for the determination of V_s in the field are very costly, and due to the rise in noise levels associated with this experiment in town areas, it is not always practical. As a result, an indirect method is utilized to calculate the V_s in laboratory. The V_s from the SPT-N value was calculated using data from 345 boreholes. Fig. 7 displays the location of the bore hole in the study region. In many cases, data collection efforts yield ground profiles that extend to a depth of up to 15 meters. However, an important criterion for categorizing a site is the average Vs within the top 30 meters of the earth. Consequently, it becomes necessary to convert the Vs at 15 meters to estimate the value at 30 meters. The shear wave's expected speed is considerably lower than its real rate. Although Vs and SA are related, high SA is produced by low shear waves. The Vs determined through calculations fulfills the majority of the necessary criteria. In this study, site class D is selected due to the Vs falling within the range of approximately 180 to 360 m/s at a depth of 30 m. The Vs has been linked to the acceleration that occurs on the surface of the ground as a result of the earth's shaking. The intensity of PGA varies depending on the location. The PGA value is influenced by several factors, including the earthquake's magnitude, the distance between the hypocenter and the soil, and the shear wave velocities. Research information is obtained from the USGS's Earthquake Catalog, which includes earthquakes with a magnitude of 4.0 or higher that took place within a 500-kilometer radius of Bogura (latitude: 24.848, longitude: 89.373) between the years 1915 and 2023 (a span of 108 years) [53].

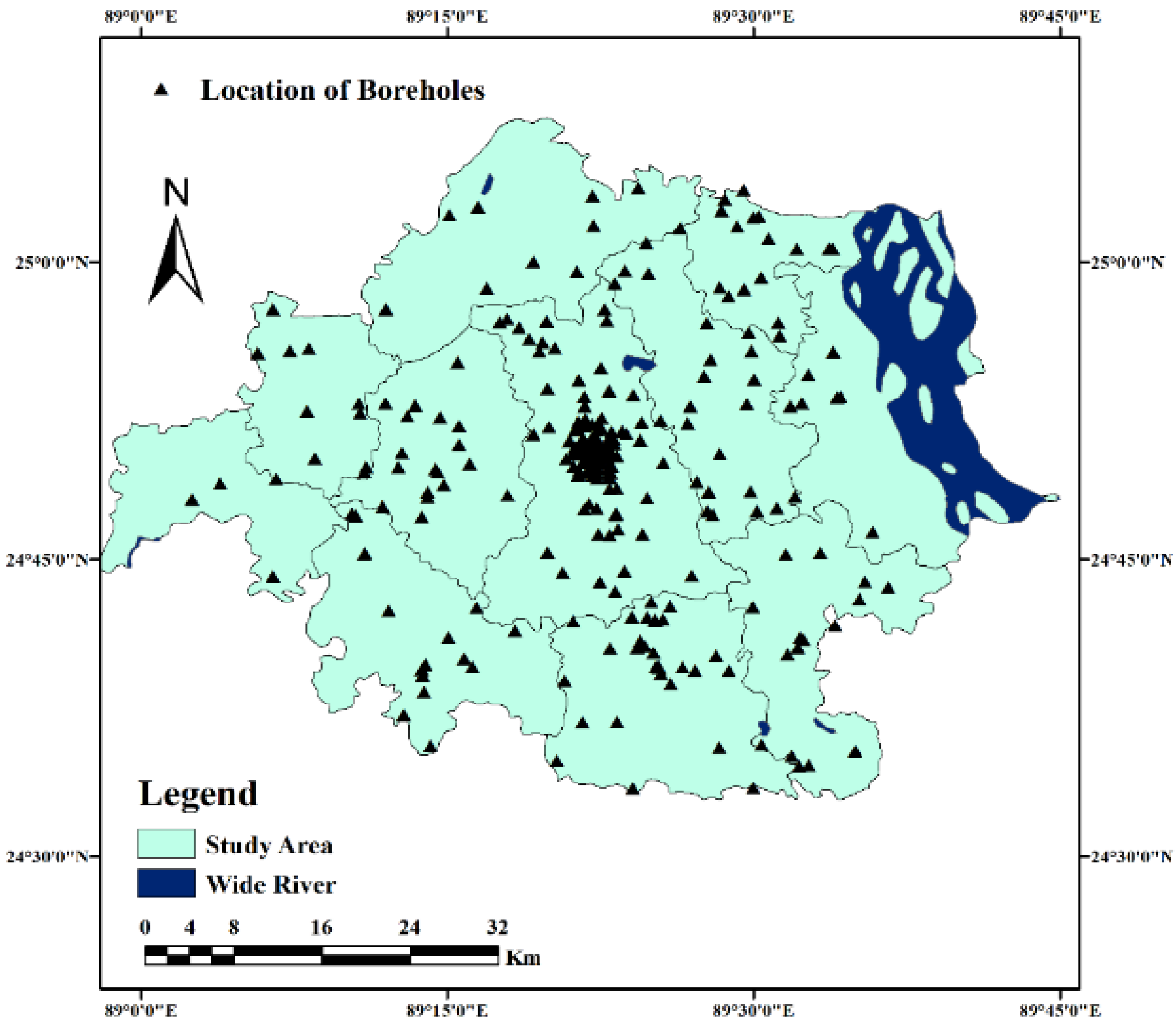

Fig. 7. Location of borehole.

The earthquake's date and time, earthquake center coordinates, depths, and magnitude are various parameters of these data. The calculated intensity of the PGA for the studied region is shown in Fig. 8. The surface-level PGA and the bed-level PGA are different from one another. To get an AF that can convert the PGA value to the SA, an equation is therefore required. Two equations are used to generate the surface acceleration, and the larger AF is chosen. The larger AF value for the Bogura district is shown in Fig. 9.

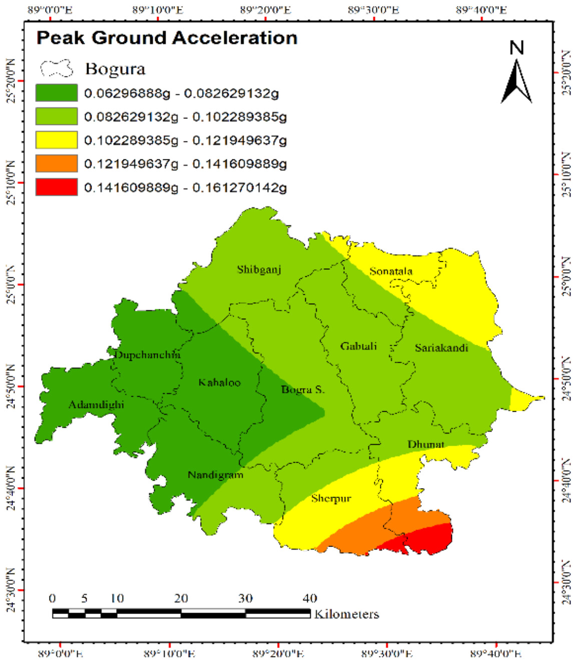

Fig. 8. PGA value for each grid point (1km X 1km) of Bogura district.

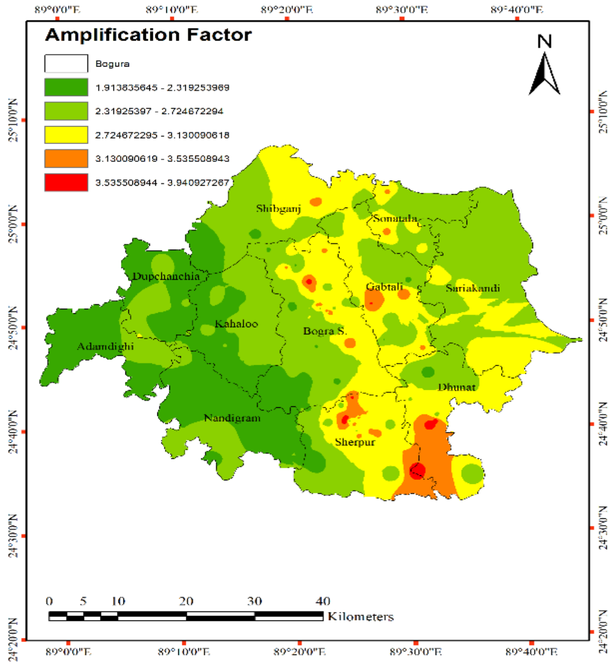

Fig. 9. Maximum AF value for each grid point (1km X 1km) of Bogura district.

With regard to the earthquake's magnitude (4.0 Mw), which will occur within a 500 km radius of Bogura (latitude: 24.848, longitude: 89.373) and last for 108 years, the distribution of areas with PGA is as follows: 28.81% of the areas have PGA between 0.062 g and 0.082 g, 49.76% have PGA between 0.082 g and 0.102 g, 16.58% have PGA between 0.102 g and 0.121 g, and 3.31% have PGA between 0.121 g and 0. According to the findings, the distribution of regions with AF is as follows: 23.34% have AF values ranging from 1.92 to 2.32, 41.87% have AF values ranging from 2.32 to 2.72, 30.28% have AF values ranging from 2.72 to 3.13, 4.14% have AF values ranging from 3.13 to 3.53, and 0.37% have AF values ranging from 3.53 to 3.78.

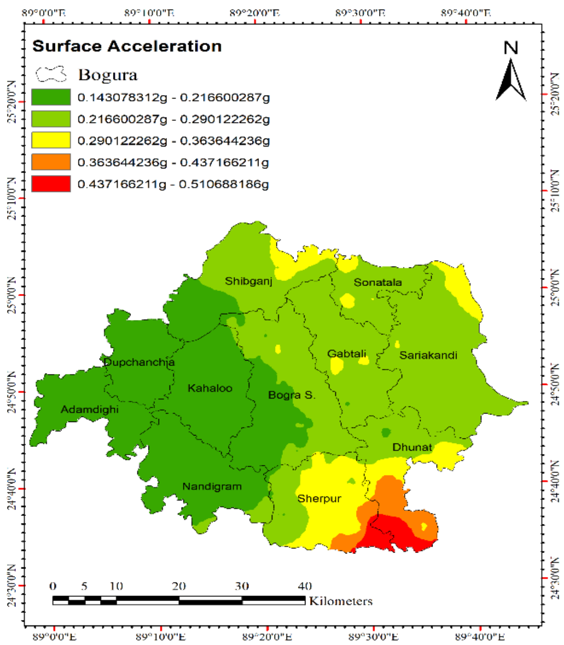

Fig. 10. SA value for each grid point (1km X 1km) of Bogura district.

The results also indicated that the conversion of PGA to SA has an impact on 37.53% of SA (0.143g–0.216g), 47.23% of SA (0.216g–0.29g), 10.60% of SA (0.29g–0.36g), 2.85% of SA (0.36g–0.43g), and 1.79% of SA (0.437g–0.51g). Additionally, 22.45% of the areas with MMI VII, 72.9% of the regions with MMI VIII, and 4.65% of the areas with MMI IX will be impacted by the conversion of SA to MMI.

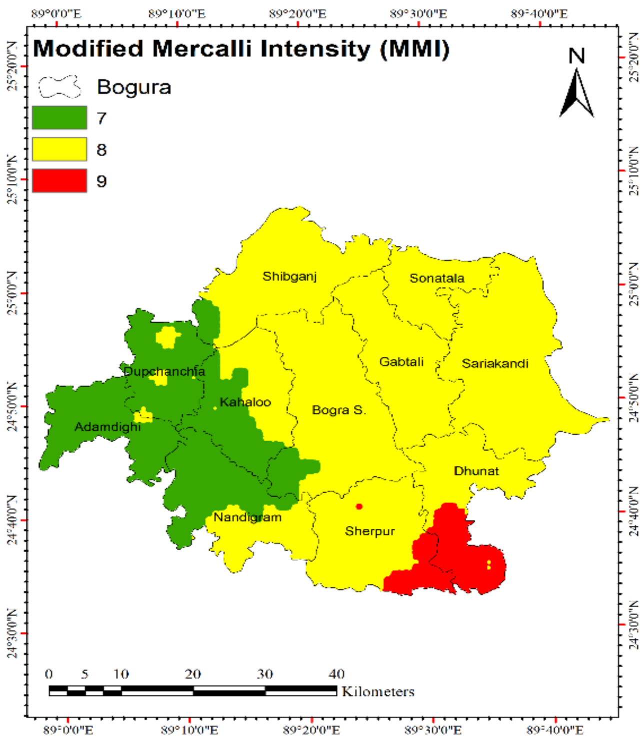

Fig. 11. MMI value for each grid point (1km X 1km) of Bogura district.

The SA values for each grid point (1km x 1km) in the Bogura district are shown in Fig. 10. The largest value is selected from the two equations for AFs. On the Earth's surface, the impact of an earthquake is referred to as intensity. There are a variety of severity levels depending on reactions, including waking, shifting furniture, chimney damage, or destruction. Currently, the Modified Mercalli Intensity Scale is widely used. MMI determines the seismic hazard for the town of Bogura. The MMI scale is a single integer; hence, the number in the current research is rounded to 0.5. The MMI intensity is shown in Fig. 11 for each grid point (1 km x 1 km) in the Bogura area.

4.2. GIS modeling of FOS, LPI and PG

The empirical procedure was used to measure the liquefaction vulnerability of Bogura District, Bangladesh. The findings have been presented through GIS modeling of LPI, FOS, and PG. These maps will offer valuable knowledge to urban planners and the general public about how to reduce liquefaction geohazards. Consequently, these maps serve as a valuable tool for disaster mitigation and management. Additionally, contour maps have been developed to depict the fluctuation of FOS values across the city. These contour lines indicate areas with equivalent FOS values and provide insight into the increase or decrease of FOS as one moves inward or outward within the region.

4.2.1. FOS distributions

An assessment of the potential for liquefaction in the Bogura district was conducted, resulting in the development of LPI maps. Each borehole's potential for liquefaction was evaluated using the value of FOS. Fig. 12 shows the variation of FOS values for each borehole at various depths. Boreholes with FOS values over 1.2 are protected against liquefaction since they don't have any liquefaction potential. The thick red line in the graph indicates the safe area's perimeter, while the blue line shows the average FOS values.

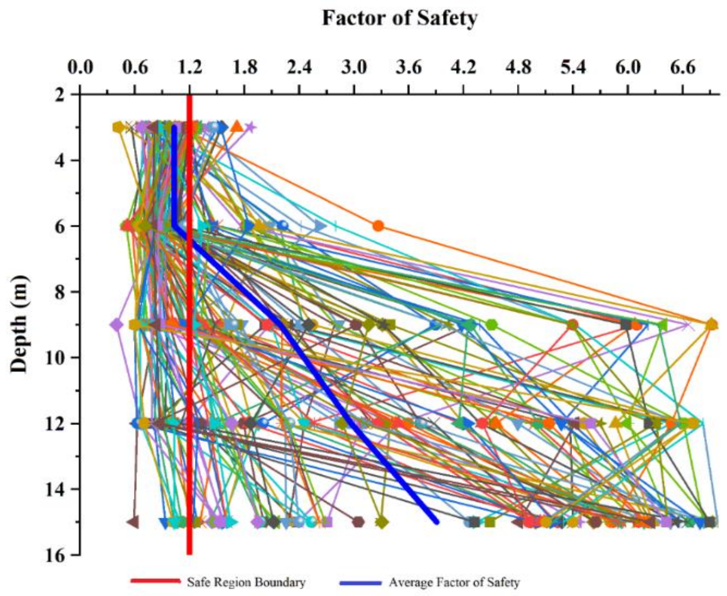

Fig. 12. Dimensional distribution of FOS values for the Bogura district.

It is clear in the Bogura district that the liquefaction potential is greater at the surface and reduced with depth. Because the soil underlying the structures has not been sufficiently improved using ground improvement techniques to prevent liquefaction, liquefaction of the topsoil might result in damage to or failure of the structures. The average FOS values are at their lowest at depths of 3 m and 6 m, indicating a significant likelihood of liquefaction. The average FOS values rise below these depths.

4.2.2. Spatial distribution of FOS

The FOS against liquefaction at various depths for BH 14 is sampled in **Table 2** using the techniques stated above. There is much disagreement among scientists as to whether soil may liquefy until FOS = 1.2. Sonmez [54] was stated that soils could be liquefied up to the range of 1 < FOS < 1.2. Based on the FOS values, the hazard level in the Bogura District has been classified as follows:

- ✓ FOS > 1.2: Safe condition
- ✓ 1.0–1.2: Moderate hazard level, indicating a high likelihood of liquefaction
- ✓ FOS < 1.0: High hazard

In Fig. 13a-e, interpolated maps representing the spatial distribution of FOS values of the research region at depths of 3, 6, 9, 12, and 15 m are displayed. ArcGIS software was used to create the FOS and liquefaction potential maps of the research areas. The standard Kriging interpolation approach was used on all maps. These maps for liquefaction danger show the potential for liquefaction in various soil layers for an earthquake of the expected size. It was discovered that the locations are liquefiable at shallow depths. The maps provide clear evidence of a decrease in liquefaction potential as depth increases. It is imperative to identify the soil layer that is most susceptible to liquefaction in order to assess the level of risk accurately.

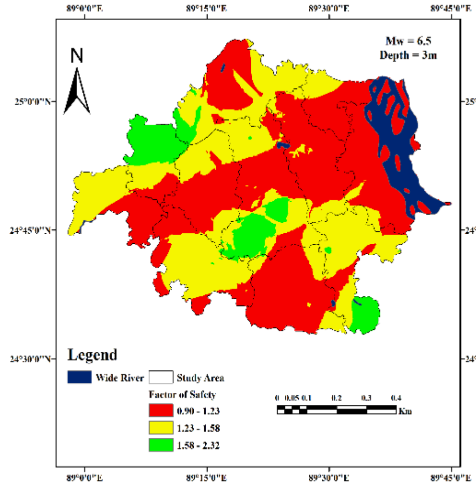

(a)

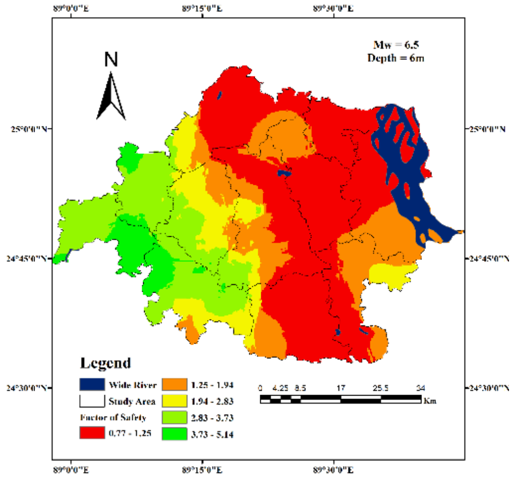

(b)

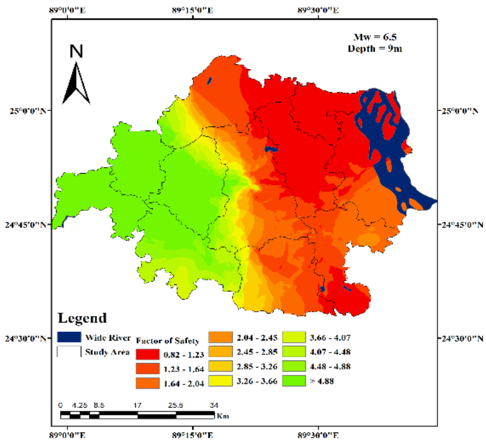

(c)

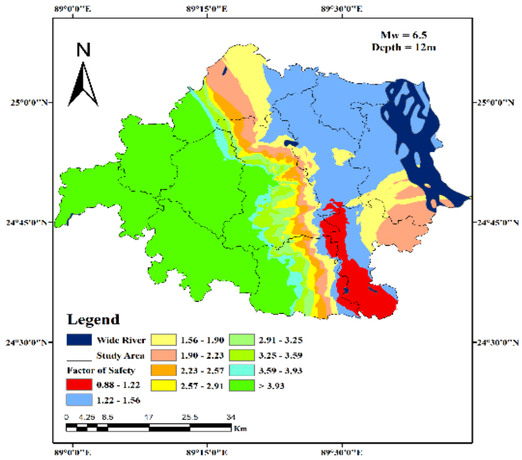

(d)

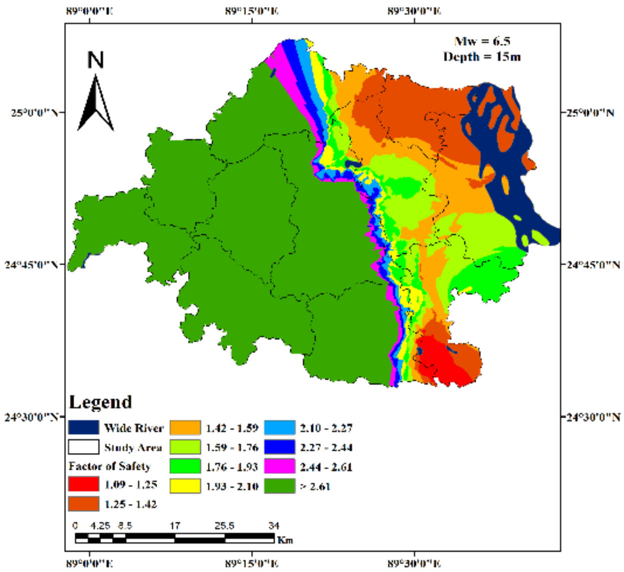

(e)

Fig. 13. Hazard zonation maps for Mw = 6.5 (a) at 3m depth, (b) at 6m depth, (c) at 9m depth, (d) at 12m depth, (e) at 15m depth.

Fig. 12 demonstrates that the average factor of safety (FOS) values in the study area reach their minimums (less than 1.2) for most of the borehole locations at depths of 1.5, 3, and 6 m, indicating a high susceptibility to liquefaction. The red colors of the legends in Fig. 13a–e also depict the minimal FOS (less than 1.2). For depths of 1.5, 3, and 6 m, red color occupies most of the research region. As shown in Fig. 13a, the FOS values for Mw = 6.5 at 3 m deep below the surface were calculated using soil data from several places in the research region using the deterministic approach. For Mw = 6.5, about 55.12% of the study region's FOS is less than 1.2, indicating liquefaction risks. A 36.07% FOS range of 1.2 to 1.58 and an 8.81% FOS range of 1.58 to 2.32 suggest that there is no chance of liquefaction in such areas. Fig. 13b–e show liquefaction probability zonation maps for Mw = 6.5 at depths of 6, 9, 12, and 15 m below the surface, respectively, with 55.03%, 73.96%, 95.11%, and 98.37% of the study zone designated as safe. The study's danger maps demonstrate that as soil depth below ground level rises from 9 to 15 m, the soil strata become less liquefiable.

4.2.3. LPI map

An example LPI calculation is shown in Table 3, and the study area's LPI zonation maps were created using the LPI values for all 345 boreholes and the Mw=6.5 earthquake magnitude. Fig. 14 displays the LPI's geographical distribution.

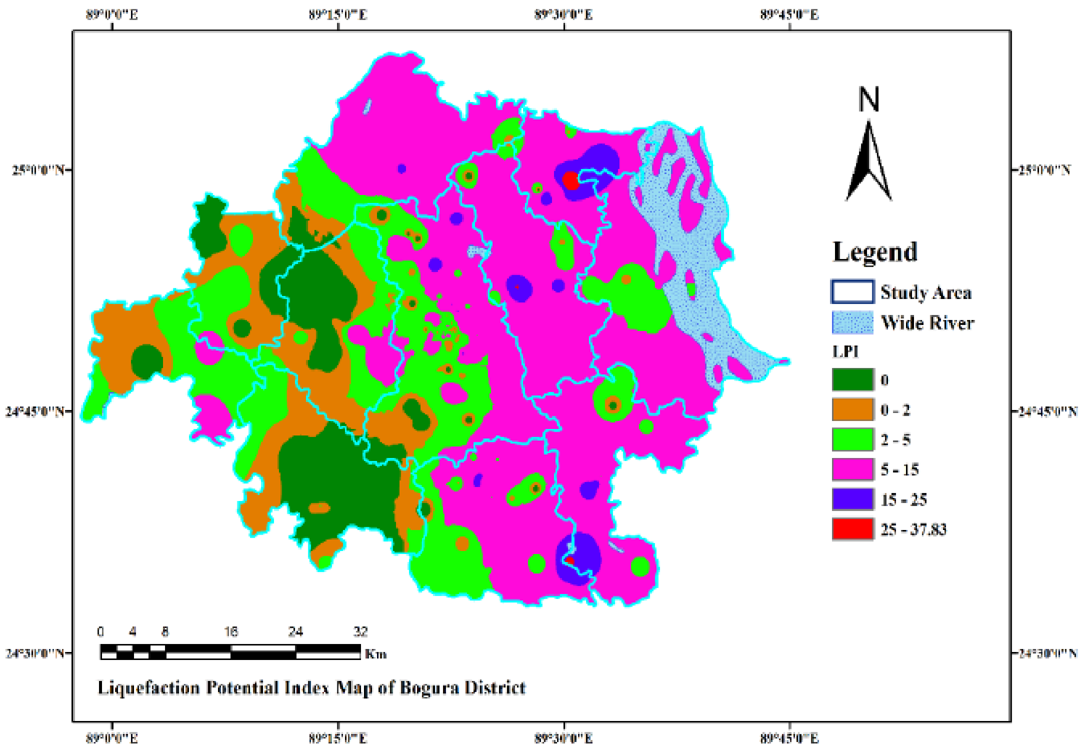

Fig. 14. LPI map of Bogura for M_w= 6.5.

In areas where the LPI exceeds 15, the occurrence of severe liquefaction is more probable, while locations with an LPI value below 5 are unlikely to experience such events [33][54]. The created maps are examined for additional interpretation, and Fig. 15 compares the proportion of study area sites that fall inside each of the different liquefaction susceptibility zones.

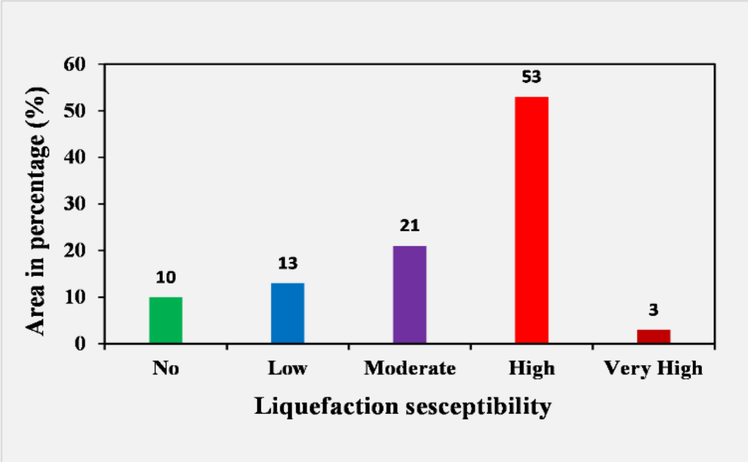

Fig. 15. Area in (%) of liquefaction susceptibility for Mw = 6.5.

According to the comparison study, 3% of the sample region is located in a zone with a very high potential for liquefaction due to earthquakes of magnitude Mw = 6. For the aforementioned earthquake scenarios, 53% of the sample territory is situated in a high liquefaction hazard area, while the remaining 21%, 13%, and 10% area may be categorized as a moderate, low, or nil liquefaction hazard, respectively.

4.2.4. PG mapping

Fig. 16 illustrates the PG map of Bogura district for the seismic scenario of Mw = 6.5 based on the interpolation approach. The calculation procedure for each location is tabulated in Table 3. The region highlighted in red signifies a zone of significant risk, whereas the dark cyan area represents a zone of minimal risk. Analysis reveals that the central and eastern sectors of the Bogura exhibit a moderate vulnerability to ground failure in comparison to the western regions.

Table 2. Sample FOS calculation using for Mw = 6.5 of BH14.

Depth of Borelog From	To	$(N_1)_{60}$	$(N_1)_{60CS}$	C_N	σ_v (kN/m^2)	σ'_v (kN/m^2)	r_d	CSR	CRR	MSF	$CRR_{7.5}$	FOS
0.0	1.5	6	11.61	1.70	24.45	24.45	0.989	0.18	0.14	1.14	0.12	0.82
1.5	3	12	17.41	1.70	49.5	34.785	0.966	0.25	0.20	1.14	0.17	0.81
3	4.5	10	15.97	1.49	74.55	45.12	0.941	0.28	0.18	1.14	0.16	0.66
4.5	6	16	21.56	1.33	100.35	56.205	0.913	0.29	0.25	1.14	0.22	0.87
6	7.5	22	26.57	1.21	127.05	68.19	0.883	0.29	0.38	1.14	0.33	1.26
7.5	9	29	31.73	1.11	154.95	81.375	0.851	0.29	0.70	1.14	0.61	2.39
9	10.5	24	26.61	1.03	182.4	94.11	0.819	0.28	0.38	1.14	0.33	1.32
10.5	12	23	26.11	0.97	210	106.995	0.787	0.28	0.36	1.14	0.31	1.29
12	13.5	29	31.99	0.91	238.8	121.08	0.754	0.27	0.73	1.14	0.64	2.71
13.5	15	31	33.80	0.86	268.2	135.765	0.723	0.26	1.00	1.14	0.87	3.84

The north-south central part indicates a high-risk zone, which has a PG ranging from 0.7 to 0.9. The western part of the Bogura district shows a safe region against ground failure due to an earthquake scenario of Mw = 6.5. In the research region, it has been determined that 2% of the total area is classified as being at a very high risk of experiencing ground failure caused by liquefaction during an earthquake scenario with a magnitude of 6.5. Additionally, 13% and 44% of the area within the study region are categorized as being at high and moderate risk, respectively.

Table 3. Calculation of LPI-based PG using Li et al. [34] at Thanthania hazi para, Sadar (24.8387° N, 89.3719°).

Depth (m)	FOS	F(z)	Layer Thickness, H	W(z)	F(z) * W(z)*H	LPI	PG
1.5	0.82	0.1774	1.5	9.625	2.561	10.572	0.942
3	0.81	0.1883	1.5	8.875	2.506		
4.5	0.66	0.3357	1.5	8.125	4.091		
6	0.87	0.1277	1.5	7.375	1.412		
7.5	1.27	0.0000	1.5	6.625	0		
9	2.39	0.0000	1.5	5.875	0		
10.5	1.32	0.0000	1.5	5.125	0		
12	1.30	0.0000	1.5	4.375	0		
13.5	2.71	0.0000	1.5	3.625	0		
15	3.85	0.0000	1.5	2.875	0		

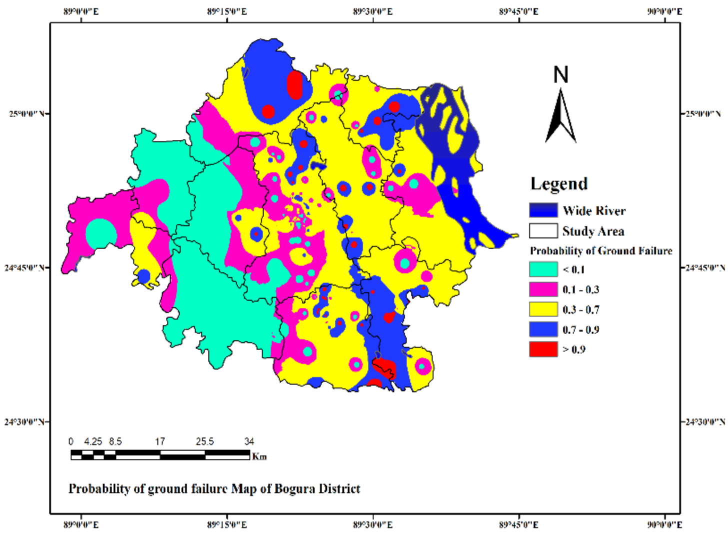

Fig. 16. PG map of Bogura for Mw=6.5.

Conversely, 21% of the area are identified as no risk. These findings align with the previous results obtained through the analysis of FOS and LPI. (See Fig. 17 for a visual representation of these results.) Fig. 18 displays a graph of Equation (15) alongside the data points (PG, LPI) acquired through the previously described procedure. It is important to note that there are numerous discrete data points where PG equals 1 or 0. This can be attributed to the fact that the intersection of the "failure" group and the "no failure" group only occurs within the LPI range of 2 to 12.

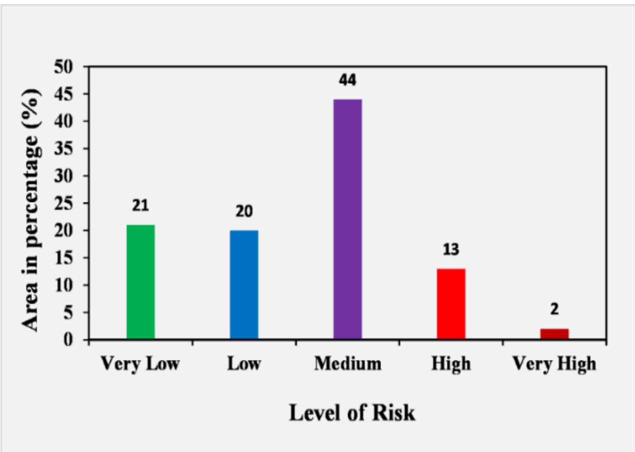

Fig. 17. Area in (%) of the degree of risk according to PG for Mw = 6.5.

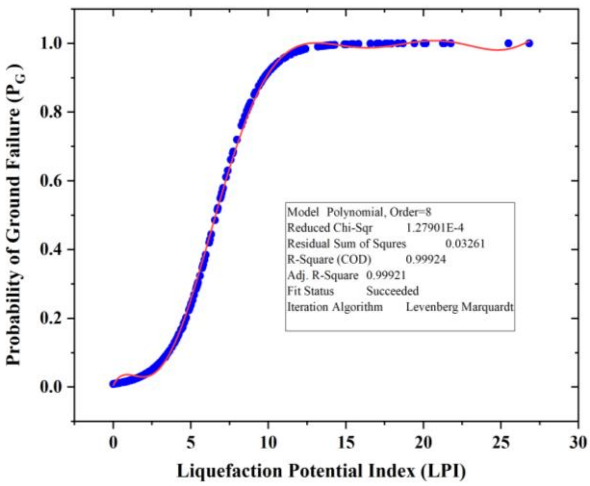

Fig. 18. Relationship between PG and LPI.

Consequently, all cases with LPI values greater than 12 would have PG equal to 1, while all cases with LPI values less than 2 would have PG equal to 0. Despite achieving a high coefficient of determination (R^2) in the curve-fitting process, certain discrete data points deviate significantly from the regression curve. Equation (22) allows for the interpretation of the PG, in relation to a specific limit state probability index (LPI) obtained from Equation (20). This interpretation is based on the deterministic model of FOS, which incorporates Equations (15) and (18). This article briefly discusses the importance of the PG-LPI mapping function, which describes the link between the estimated LPI and the PG parameter. As shown by the findings previously provided, if the index LPI is employed directly for evaluating liquefaction risk, a separate set of criteria must be pre-calibrated for a distinct deterministic model of FOS that is put into Eq. (20). This supports the earlier findings that Lee et al. [11] published. The possibility of liquefaction-induced ground failure, in contrast to LPI, offers a "uniform platform" for evaluating liquefaction risk.

5. Conclusions

The geotechnical devastation caused by seismic risks has been catastrophic. Bogura District was impacted by the 7.8-magnitude earthquake that struck Nepal in 2015 and the 6.0-magnitude earthquake that struck Dhekiajuli, Assam, India, in 2021. In addition, many earthquakes of minor to medium size have recently affected the Bogura district. Although the Bogura district is seismically sensitive, there is no Mercalli intensity risk map for seismicity. In the present investigation, an intensity map was generated utilizing universally applicable equations. To create a final intensity map, SA, AF, and PGA were calculated, and the numerical value was represented using GIS. According to the developed Mercalli intensity spatial distribution map, intensities VII and IX will have an influence on the majority of the research region. This is an indication of massive harm in the construction of the Bogura.

Additionally, the current study is the first of its type to assess the PG due to soil liquefaction in the Bogura District. To calculate the PG, the susceptibility of liquefaction phenomena in the subsurface stratum of the research region was determined in terms of FOS and LPI. Then the numerical values of FOS and LPI were visualized utilizing GIS. Depending on their color designation, red denotes extremely dangerous areas, while green denotes areas that are safe from liquefaction. As soil depth below ground level increases from 9 to 15 meters, the vulnerability of soil liquefaction reduces, according to the spatial interpolation maps produced for the study. This may be explained by the increased overburden pressure to which the soil layers above and below are subjected, resulting in soil rigidity. The liquefaction hazard maps indicate that a majority of locations in the study area, especially in the central and eastern regions, are at high risk of experiencing liquefaction. The quantitative characteristics of the liquefiable strata are depicted in the subsequent map, which shows the likelihood of ground failure. This map also highlights the specific area where ground failure resulting from liquefaction is most probable. The majority of the research area has a medium-to-high likelihood and danger of ground failure, according to the findings. For the planning and design of any construction, including moderate-to-tall buildings, the Mercalli risk map and the spatial interpolation PG map may be utilized as sources of information.

Funding

This research was funded by the Institute of Research and Training (IRT), Hajee Mohammad Danesh Science and Technology University, Bangladesh. Reference No.: HSTU/IRT/3869(75).

Conflicts of interest

The authors declare no conflict of interest.

Authors contribution

Md. Belal Hossain: Conceptualization; Supervision; Project administration; Data analysis; Original draft writing; Review & editing.

Md. Mahabub Rahman: Data curation; Methodology; Formal analysis; Software; Validation; Visualization; Writing – original draft.

Abbreviations	
Shear Wave Velocity	Vs
Amplification Factor	AF
Peak Ground Acceleration	PGA
Surface Acceleration	SA
Probability of Ground Failure	PG
Liquefaction Potential Index	LPI
Factor of Safety	FOS

References

[1] Ansa A, Biro Y, Erken A, Gülerce Ü. Seismic Microzonation: A Case Study. Recent Adv. Earthq. Geotech. Eng. Microzonat., Dordrecht: Kluwer Academic Publishers; n.d., p. 253–66. doi:10.1007/1-4020-2528-9_9.

[2] Dai FC, Lee CF, Zhang XH. GIS-based geo-environmental evaluation for urban land-use planning: a case study. Eng Geol 2001;61:257–71. doi:10.1016/S0013-7952(01)00028-X.

[3] van Rooy JL, Stiff JS. Guidelines for urban engineering geological investigations in South Africa. Bull Eng Geol Environ 2001;59:0285–95. doi:10.1007/s100640000076.

[4] T. G. Sitharam, P. Anbazhagan. Seismic microzonation: principles, practices and experiments. Int. Conf. Dev. Urban Areas Geotech. Eng. , Saint Petersburg, USA, Saint Petersburg., 2008.

[5] Behzadfar, B., Maleki, A., Lotfollahi Yaghin MA. Improved Seismic Performance of Chevron Brace Frames Using Multi-Pipe Yield Dampers. J Rehabil Civ Eng 2020;8:137–55.

doi:10.22075/jrce.2020.19792.1383.

[6] Rezaee Manesh, M., Fattahi, S., & Saffari H. Investigation of Earthquake Significant Duration on the Seismic Performance of Adjacent Steel Structures in Near-Source. J Rehabil Civ Eng 2021;9:84–101. doi:10.22075/jrce.2020.20373.1410.

[7] Tehrani, P., Eini A. Seismic Performance Assessment of Steel Moment Frames with Non-parallel System Irregularity. J Rehabil Civ Eng 2022;10:109–28. doi:10.22075/jrce.2021.23918.1528.

[8] Jalilkhani M, Babaei M, Ghasemi SH. Evaluation of the seismic response of single-story RC frames under biaxial earthquake excitations. J Rehabil Civ Eng 2020;8:98–108. doi:10.22075/JRCE.2020.19727.1379.

[9] Mostazid, M. I., Mahabub, M. and Mahbur M. Seismic Vulnerability Assessment of Existing RCC Buildings in Dinajpur City : A Case Study on Ward No . 6. 2rd Int. Conf. Planin. Archit. Civ. Eng., 2019, p. 1–6.

[10] Hoseynzadeh, H., Mortezaei A. Seismic Vulnerability and Rehabilitation of One of The World's Oldest Masonry Minaret under The Different Earthquake Frequency Contents. J Rehabil Civ Eng 2021;9:12–36. doi:10.22075/jrce.2021.21251.1441.

[11] Lee DH, Ku CS, Yuan H. A study of the liquefaction risk potential at Yuanlin, Taiwan. Eng Geol 2004;71:97–117. doi:10.1016/S0013-7952(03)00128-5.

[12] Idriss IM, Boulanger RW. Semi-empirical procedures for evaluating liquefaction potential during earthquakes. Soil Dyn Earthq Eng 2006;26:115–30. doi:10.1016/j.soildyn.2004.11.023.

[13] Setiawan H, Serikawa Y, Sugita W, Kawasaki H, Miyajima M. Experimental study on mitigation of liquefaction-induced vertical ground displacement by using gravel and geosynthetics. Geoenvironmental Disasters 2018;5:22. doi:10.1186/s40677-018-0115-3.

[14] Verdugo R, González J. Liquefaction-induced ground damages during the 2010 Chile earthquake. Soil Dyn Earthq Eng 2015;79:280–95. doi:10.1016/j.soildyn.2015.04.016.

[15] Setiawan H, Serikawa Y, Nakamura M, Miyajima M, Yoshida M. Structural damage to houses and buildings induced by liquefaction in the 2016 Kumamoto Earthquake, Japan. Geoenvironmental Disasters 2017;4:13. doi:10.1186/s40677-017-0077-x.

[16] Sharma K, Subedi M, Acharya IP, Pokharel B. Geotechnical and Structural Aspect of 2015 Gorkha Nepal Earthquake and Lesson Learnt. J Inst Eng 2018;13:20–36. doi:10.3126/jie.v13i1.20345.

[17] Khatti J, Fissha Y, Grover KS, Ikeda H, Toriya H, Adachi T, et al. Cone penetration test-based assessment of liquefaction potential using machine and hybrid learning approaches. Multiscale Multidiscip Model Exp Des 2024. doi:10.1007/s41939-024-00447-x.

[18] Hossain MB, Roknuzzaman M, Rahman MM. Liquefaction Potential Evaluation by Deterministic and Probabilistic Approaches. Civ Eng J 2022;8:1459–81. doi:10.28991/CEJ-2022-08-07-010.

[19] Rahman MM, Hossain MB, Roknuzzaman M. Effect of peak ground acceleration (PGA) on liquefaction behavior of subsoil: A case study of Dinajpur Sadar Upazila, Bangladesh. AIP Conf. Proc., 2023, p. 030002. doi:10.1063/5.0129770.

[20] Kumar DR, Samui P, Burman A, Biswas R, Vanapalli S. A novel approach for assessment of seismic induced liquefaction susceptibility of soil. J Earth Syst Sci 2024;133:128. doi:10.1007/s12040-024-02341-z.

[21] Kumar K, Samui P, Choudhary S. Assessment of maximum liquefaction distance using soft computing approaches. Geomech Eng 2024;37:395–418. doi:https://doi.org/10.12989/gae.2024.37.4.395.

[22] Rahman M, Hossain M, Sayed A, Thakur S. Assesment of Liquefaction Potential Based on the Logistic Regression Machine Learning Algorithm. 7th Int. Conf. Civ. Eng. Sustain. Dev. (ICCESD 2024), 2024, p. 1–11. doi:10.13140/RG.2.2.24047.65440.

[23] Bhardwaj V, Singh K. Assessment of landslide susceptibility of Pithoragarh, Uttarakhand (India) using logistic regression and multi-criteria decision-based analysis by analytical hierarchy process. Appl Earth Sci Trans Institutions Min Metall 2023;132:178–86. doi:10.1080/25726838.2023.2237370.

[24] Alsabhan AH, Singh K, Sharma A, Alam S, Pandey DD, Rahman SAS, et al. Landslide susceptibility assessment in the Himalayan range based along Kasauli – Parwanoo road corridor using weight of evidence, information value, and frequency ratio. J King Saud Univ - Sci 2022;34:101759. doi:10.1016/j.jksus.2021.101759.

[25] Jalil A, Fathani TF, Satyarno I, Wilopo W. Liquefaction in Palu: the cause of massive mudflows. Geoenvironmental Disasters 2021;8:21. doi:10.1186/s40677-021-00194-y.

[26] R. W. Boulanger and I. M. Idriss. CPT and SPT based liquefaction triggering procedures. 2014.

[27] Qazi A, Singh K, Vishwakarma DK, Abdo HG. GIS based landslide susceptibility zonation mapping using frequency ratio, information value and weight of evidence: a case study in Kinnaur District HP India. Bull Eng Geol Environ 2023;82:332. doi:10.1007/s10064-023-03344-8.

[28] Singh K, Khaidem S, Gupta SK, Sharma A. Assessment of landslide occurrence and prediction of susceptible zone based on GIS along national highway 37, Manipur, India. Sādhanā 2024;49:74. doi:10.1007/s12046-023-02422-7.

[29] Gururani DM, Kumar Y, Abed SA, Kumar V, Vishwakarma DK, Al-Ansari N, et al. Mapping Prospects for Artificial Groundwater Recharge Utilizing Remote Sensing and GIS Methods. Water 2023;15:3904. doi:10.3390/w15223904.

[30] McGuire RK. Seismic Ground Motion Parameter Relations. J Geotech Eng Div 1978;104:481–90. doi:10.1061/AJGEB6.0000615.

[31] Atkinson GM, Boore DM. Modifications to Existing Ground-Motion Prediction Equations in Light of New Data. Bull Seismol Soc Am 2011;101:1121–35. doi:10.1785/0120100270.

[32] I. M. Idriss and R. W. Boulanger. Soil liquefaction during earthquakes. 2008.

[33] T. Iwasaki, K. I. Tokida, F. Tatsuoka, S. Watanabe SY and HS. Micro-zonation for soil liquefaction potential using simplified methods. 3rd Intl. Microzonat. Conf. proceeding, 1982, p. 1310–1330.

[34] D. K. Li CHJ and RDA. Liquefaction potential index: a critical assessment using probability concept. J Geoengin 2006;1:11–24. doi:https://doi.org/10.6310/jog.2006.1(1).2.

[35] Weil R, Brady N. Soil Architecture and Physical Properties. Chp. 4. Nat. Prop. Soils. 15th ed. P, 2017.

[36] H. Ali. Earthquake database and seismic zoning of Bangladesh. Inf. Technol. tools Nat. disaster risk Manag. Proc. Int. Symp., 1999, p. 59–74.

[37] Ghosh S. Geomorphic Appraisal of Active Tectonics and Fluvial Anomalies in Peninsular Rivers of the Bengal Basin (West Bengal, India), 2022, p. 503–41. doi:10.1007/978-3-030-79634-1_23.

[38] BNBC. Bangladesh National Building Code. Hous Build Res Inst 2014;Part 6(2).

[39] B. K. Bansal and S. K. Nath. Seismic micro-zonation handbook, Geoscience divisions. 2011.

[40] Yilmaz I, Bagci A. Soil liquefaction susceptibility and hazard mapping in the residential area of Kütahya (Turkey). Environ Geol 2006;49:708–19. doi:10.1007/s00254-005-0112-1.

[41] Ayele A, Woldearegay K, Meten M. A review on the multi-criteria seismic hazard analysis of Ethiopia: with implications of infrastructural development. Geoenvironmental Disasters 2021;8:9. doi:10.1186/s40677-020-00175-7.

[42] McGuire RK. Seismic Ground Motion Parameter Relations. ASCE J Geotech Eng Div 1978;104:481–90. doi:10.1061/ajgeb6.0000615.

[43] Lee SH. Regression models of shear wave velocities in Taipei basin. J Chinese Inst Eng 1990;13:519–32. doi:10.1080/02533839.1990.9677284.

[44] Dikmen Ü. Statistical correlations of shear wave velocity and penetration resistance for soils. J Geophys Eng 2009;6:61–72. doi:10.1088/1742-2132/6/1/007.

[45] Ali B. Estimation of linear site amplification by a ground motion prediction equation using results from a site survey. Pakistan J Meteorol 2013;9:33–42.

[46] Boore DM. Estimating s(30) (or NEHRP Site Classes) from Shallow Velocity Models (Depths < 30 m). Bull Seismol Soc Am 2004;94:591–7. doi:10.1785/0120030105.

[47] Boore DM, Joyner WB. Site amplifications for generic rock sites. Bull Seismol Soc Am 1997;87:327–41. doi:10.1785/BSSA0870020327.

[48] Sarker JK. GIS based methodologies of seismic Hazard and risk analysis for Bangladesh. BUET, 2011.

[49] Toni M. Simulation of strong ground motion parameters of the 1 June 2013 Gulf of Suez earthquake, Egypt. NRIAG J Astron Geophys 2017;6:30–40. doi:10.1016/j.nrjag.2016.12.002.

[50] Boore DM, Stewart JP, Seyhan E, Atkinson GM. NGA-West2 Equations for Predicting PGA, PGV, and 5% Damped PSA for Shallow Crustal Earthquakes. Earthq Spectra 2014;30:1057–85. doi:10.1193/070113EQS184M.

[51] M. D. Trifunac; A. G. Brady. On the correlation of seismic intensity scales with the peaks of recorded strong ground motion. Bull Seismol Soc Am 1975;65:139–62. doi:https://doi.org/10.1785/BSSA0650010139.

[52] Hussien MN, Karray M. Shear wave velocity as a geotechnical parameter: an overview. Can Geotech J 2016;53:252–72. doi:10.1139/cgj-2014-0524.

[53] USGS. Search Earthquake Catalog 2023.

[54] Sonmez H. Modification of the liquefaction potential index and liquefaction susceptibility mapping for a liquefaction-prone area (Inegol,Turkey). Environ Geol 2003;44:862–71. doi:10.1007/s00254-003-0831-0.